Enhanced Flexibility in Direct Laser Interference Patterning through Industrial Robot Integration

L. Olawsky[1,2*], S. Moghtaderifard[2], R. Baumann[2], D. Li[3], C. Kuhn[1], K. Du[3], M. Soldera[2], and A. F. Lasagni[2,4]

[1] *ALOtec Dresden GmbH, Zum Wiesengrund 2, 01723 Kesselsdorf, Germany*
[2] *Institute for Manufacturing Technology, Technische Universität Dresden, George-Baehr-Str. 3c, 01069 Dresden, Germany*
[3] *EdgeWave GmbH, Carlo-Schmid-Straße 19, 52146 Würselen, Germany*
[4] *Fraunhofer- Institut für Werkstoff- und Strahltechnik IWS, Winterbergstr. 28, 01277 Dresden, Germany*
[*] *Corresponding author's e-mail: olawsky@alotec.de*

Direct Laser Interference Patterning (DLIP) is a well-established method for surface functionalization, enhancing properties like friction, wetting, and bacteria repellence. Traditionally, DLIP uses transla-tional stage or scanner systems to move either the laser or the component, offering high processing velocities and precision. However, these methods face limitations with heavy 3D parts, such as form-ing tools, reducing the range of components and applications. The study presents a new DLIP ap-proach using an industrial robot, providing more freedom for treating large components with complex geometries. The DLIP tool, including the laser source, is attached to a robot arm. The laser delivers nanosecond pulses with up to 120 W power and 40 mJ pulse energies, designed to be lightweight and vibration-tolerant. The DLIP optics generate an elongated rectangular beam with a long depth of focus. Initial experiments structured stainless steel plates with a pulse frequency up to 800 Hz and 15 W power, with structuring velocities from 2 to 20 mm/s. Different structuring strategies were applied to punches, and their tribological performance in forming applications was compared to non-structured punches. The produced topographies are characterized using a confocal microscope.

DOI: 10.2961/jlmn.2024.03.2012

Keywords: direct laser interference patterning, free-form geometry, industrial robot, forming tool, friction reduction

1. Introduction

Direct Laser Interference Patterning (DLIP) is a versatile tool for processing surfaces of a wide variety of materials, such as polymers, ceramics, coatings, and metals [1-5]. By overlapping at least two coherent laser beams, an interference pattern with a high energy density can be generated [6]. This leads to local melting, ablation or modification of the material surface at the interference maxima positions, forming homogeneous microstructures with feature sizes down to the sub-µm range [7-9]. These periodic surface patterns can enhance or control different properties such as friction, corrosion, wetting, and biocompatibility [10-13].

While the surface properties are controlled by the geometry and size of the produced structures, both throughput and processability of 3D parts are defined by the type of the utilized positioning equipment. High-precision and fast parallel kinematics, such as linear stages, are used to control the position of both the laser head and the workpiece [14]. The motion during the process is carried out almost exclusively by the movement of the workpiece. Movement of the laser processing tool (optical head) only occurs when structuring rotationally symmetrical components or adjusting the working distance [15,16]. Scanner system (with galvanometer or polygon mirrors) can be also used without the need to move the workpiece or the process head [17,18]. However, the working area is limited, typically to a few hundreds of millimeters (e.g. 300 × 300 mm²). In addition, the small number of axes, and therefore the low number of degrees of freedom (DOF), limits the complexity of the workpieces that can be processed either on flat surfaces or cylinders.

In order to structure complex 3D surfaces, a positioner with a higher number of DOF is required. For instance, hexapods with six DOF enable fast and precise fabrication of structures on 3D surfaces [19]. However, hexapods are also characterized by limited load capacities and a small working area. Serial kinematics, such as industrial robot arms, close this gap by providing a high number of axes and a larger working range compared to hexapods [20]. Furthermore, robot systems can be equipped with additional peripheral axes, which further increases the DOF. However, robot systems have lowered stiffness and poor positioning accuracy in comparison with parallel kinematics [21,22].

In case of DLIP, when using high velocity translational stages combined with laser sources having average powers over ~ 200 W, process throughputs of 1 m²/min could be already achieved [23]. Furthermore, combining a DLIP module with a polygon scanner system, polymer surfaces could be also treated with a ps-pulsed laser source, reaching a throughput of 1.1 m²/min [24]. Using a hexapod system, spherical parts could be also recently processed using DLIP, but only in areas of few cm² as well as parts having less than 1 Kg in weight [19]. Related to the implementation of robot system in combination with DLIP, fundamental investigations were performed using a UV laser source (263 nm, ~4

ns pulses) delivering ~ 20-30 µJ of pulse energy [25]. This setup included a DLIP optics with a depth of focus on only ~100-150 µm. Although it was possible to treat cylindrical parts of polyethylene terephthalate (PET), the system showed strong limitations due to the very short depth of focus and the limited pulse energy provided by the laser source. Thus, further improvements are still necessary, in particular for treating large and heavy 3D metallic components.

Among the plethora of potential applications in which versatile DLIP processing on complex 3D parts can be applied (for instance implants or bearings), this work was motivated by the need of functional tools for sheet metal forming [26,27]. The sheet metal processing industry primarily uses complex and heavy tools for its forming process. These tools are subject to constant friction and wear and are limited in terms of their service life [28,29]. Lubricants are thus utilized to minimize interface forces between tools and workpieces, leading to a potential reduction of up to 30% in the coefficient of friction (COF) [30]. However, the use of lubricants is associated with higher efforts. For instance, the formed metallic parts have to be freed from lubricant residues and re-dried, which is economically and ecologically inefficient [31,32]. Consequently, the industrial sector as well as the scientific community are actively pursuing lubricant-free forming processes, also known as dry forming, by developing special coatings that replicate lubricant properties [33,34]. Furthermore, these coatings must be structured in order to further reduce the COF [35].

This work involves transferring the DLIP process from parallel kinematics to a robot system to structure tools for metal forming. For this purpose, a laser module including the laser source and a special DLIP optics (ELIPSYS®, SurFunction GmbH/TU Dresden), with a high depth of focus, is flanged to an industrial robot arm. This enables the structuring of complex geometries through its high DOF. To achieve this, a new strategy for fabricating the periodic structures is developed. Finally, punches used in forming processes are structured and subjected to forming tests. In particular, it is also evaluated the impact of possible non-homogeneities in the tribological performance of the treated parts. This approach opens up new application possibilities for the DLIP process, including complex 3D functional components.

2. Material and methods

In the preliminary tests, two setups utilizing parallel and serial kinematics were employed to fabricate DLIP structures on stainless steel plates (AISI 304). The parallel kinematics workstation (developed in-house at TU Dresden, Germany) features an infrared nanosecond laser (IS400-3-GH, EdgeWave GmbH, Germany) and a two-beam DLIP optics system (ELIPSYS, SurFunction GmbH, Germany).

The laser source emits pulses with a Gaussian distribution, a duration of 7 ns and a maximum pulse energy of 40 mJ, operating at a maximum pulse frequency f of 5 kHz. The resulting spot using this optical configuration has an elliptical shape measuring approximately 2700 µm × 120 µm (length × width) with a focal depth of approximately 10 mm. The working distance between the optics and the component surface was approximately 78 mm. The spatial period Λ of the interference pattern, and thus of the produced texture, was set to 10 µm. The linear x-y positioning stages (PRO225LM and PRO280LM, Aerotech GmbH, Germany) providing two degrees of freedom, offer a travel length of 500 mm, and are calibrated with an accuracy of ±1.0 µm and ±2.5 µm, respectively.

In contrast, the serial kinematics workstation (ALOstation, ALOtec Dresden GmbH, Germany) is equipped with a similar infrared nanosecond laser (RX400-1-L, EdgeWave GmbH, Germany) and the aforementioned two-beam DLIP optics. This laser source also provides a Gaussian beam with a pulse energy of up to 40 mJ, a duration of 7.5 ns and a maximum pulse frequency of 10 kHz. Both the laser source and optics are directly integrated and attached to the 6-axis robot (KR90 R3100 HA, KUKA AG, Germany), capable of handling a maximum payload of 90 kg within a working range of 3095 mm. The positioning accuracy is defined at ±50 µm. In addition to the robot system, an external turn-tilt axis is integrated. The robot is programmed online using a control system (ROBOTstarVI, Reis Robotics GmbH, Germany).

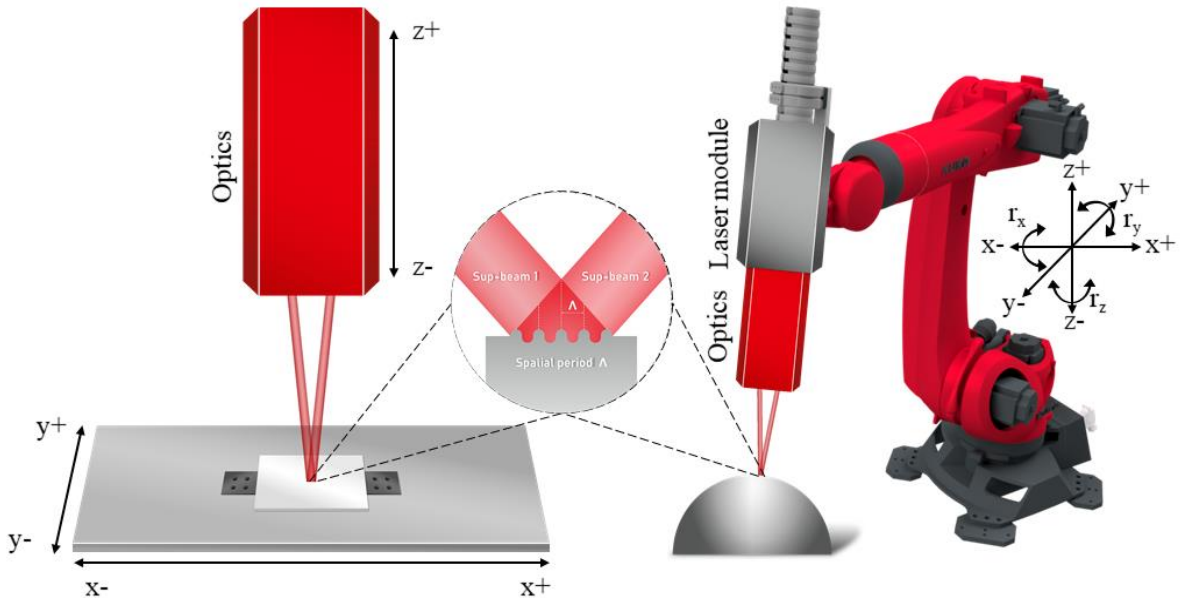

Fig. 1 Schematic illustration of the experimental set-ups; left: parallel kinematics with three axes, right: serial kinematics with six axes.

Both the media and data supply of the laser are managed through an energy chain. Schematic representations of the parallel and serial kinematics workstations are provided in Fig. 1.

The topography of the textured surfaces was subsequently analyzed using a confocal microscope (S Neox 3D Surface Profiler, SENSOFAR TECH, Spain) and a scanning electron microscope (ZEISS GeminiSEM 300, Carl Zeiss AG, Germany). The homogeneity H of the depth of the fabricated textures is evaluated using the Gini coefficient G, following the methodology outlined in [36,37]. The Gini coefficient, originally developed as a statistical measure of income inequality. In surface structuring, it quantifies the homogeneity of a property within the repeating elements of a periodic pattern. Its value ranges from 0 (uniformity) to 1 (inequality). By employing Fourier analysis to isolate periodic features, the Gini coefficient serves as an objective tool for assessing the consistency of the structuring process, supporting surface quality evaluation and process optimization.

Final forming tests were conducted on a sheet metal test machine (BUP600, ZwickRoell GmbH & Co. KG, Germany) with a maximum force of 600 kN. For this purpose, rounded punches with a diameter of 100 mm were manufactured from mild steel (comparable to AISI 1024) and used to form aluminum sheets with a thickness of 0.9 mm.

3. Results and discussion

To investigate the characteristics of the robot-based DLIP structuring process, an initial examination was conducted using single laser pulses. As mentioned before, this pulses have an elongated geometry and within them the interference pattern can be found. The individual pulses were fired with increasing laser fluence and the resulting modified area as well as the depth of the DLIP line-like features were measured.

Examples of confocal microscopy images of irradiated spots for laser fluence levels Φ of 2.6 J/cm², 4.7 J/cm², and 5.6 J/cm² are depicted in Fig. 2a-c. Detailed images of each spot are provided in Fig. 2d-f, respectively. At the lowest used laser fluence of 2.6 J/cm² (Fig. 2a,d), an ablated area of approximately 1250 µm × 33 µm is observed. The decrease in structure depth at the spot edges can be attributed to the intensity profile of the laser beam. At 4.7 J/cm² (Fig. 2b,e), the laser-modified area enlarges to 2150 µm × 68 µm, and at 5.6 J/cm² (Fig. 2c,f), it further increases to 2300 µm × 78 µm. In addition, at Φ = 5.6 J/cm², the patterned structure shows deterioration at the center of the ablation area, where the intensity density is highest due to the Gaussian distribution. The grooves between the peaks become re-filled with molten and re-solidified material as a result of the excessively high deposited energy, as shown in Fig. 2f, a phenomenon previously discussed in [38,39].

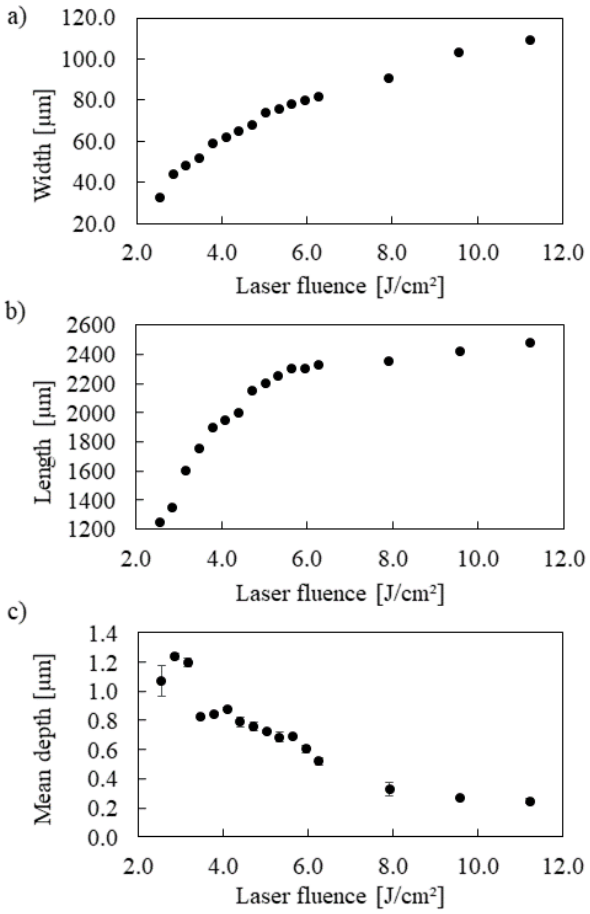

Fig. 3 Ablation spot width (a), length (b) and mean depth (c) depending on the laser fluence.

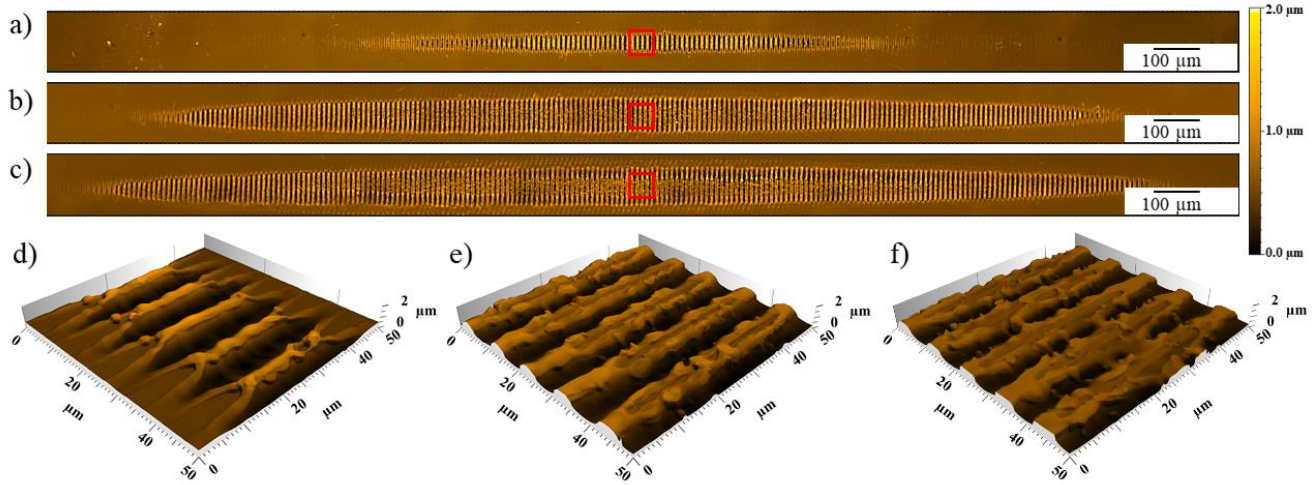

Fig. 2 Confocal microscope measurements of DLIP structured stainless steel showing total spot dimension (a-c) and details (d-f); (a, d): Φ = 2.6 J/cm²; (b, e): Φ = 4.7 J/cm²; (c, f): Φ = 5.6 J/cm².

Fig. 3 illustrates the measured ablated spot width, length, and average structure depth as a function of the laser fluence. As expected, an increase in laser fluence results in a larger laser modified areas (Fig. 3a,b) within the irradiated zone. Conversely to the area dimensions, the average structure depth decreases with increasing laser fluence (Fig. 3c), as in the used fluence range excessive melting occurs due to the high energy density. Comparable structural depths could be achieved in 3D surfaces (sphere) using a hexapod platform and a ps-laser [19].

Knowing the dimensions of the ablated area as function of the fluence is critical for high-quality and full-surface structuring, since they have to be used to determine both the pulse-to-pulse distance (in the direction of movement of the laser spot) as well as the hatch distance (lateral distance between produced DLIP-tracks).

In this way, by slightly overlapping the laser pulses in both directions, large uninterrupted areas can be treated. Furthermore, once the laser fluence is determined, and thus the needed pulse energy, the process throughput can be controlled by changing the frequency f (repetition rate) of the laser source. Then, the process velocity v can be linked to the pulse-to-pulse distance d_{p2p}, according to Equation 1.

$$f = v/d_{p2p}. \quad (1)$$

In case of a laser fluence $\Phi = 4.7$ J/cm², the measured spot width (from Fig. 3) is 68 µm (d_{p2p}). By considering a process velocity v of 2.5 mm/s, then the calculated pulse frequency was 37 Hz. An optical microscope image of large-area produced line-like DLIP structure at the above mentioned parameters is shown in Fig. 4a. As it can be seen, the produced topography reveals minimal gaps between the individual pulses which means that the surface was not totally homogeneously treated, represented by the calculated homogeneity H of 0.66. A possible explanation for this behavior could be the inconsistent process velocity of the robot, which is reinforced by vibrations in the optics and laser source. At the same time, it has to be considered that the intensity of the interference maxima positions varies within the laser spot that can also explain the observed results. Thus, for a better coverage of the textured area the distance d_{p2p} between the laser spots has to be reduced, which means that the frequency f of the laser source has to be increased.

Therefore, further experiments were conducted at 45 Hz and 50 Hz, corresponding to d_{p2p} distances of 56 and 50 µm, respectively. The produced topographies and calculated homogeneities are shown in Fig. 4b and 4c. As it can be seen,

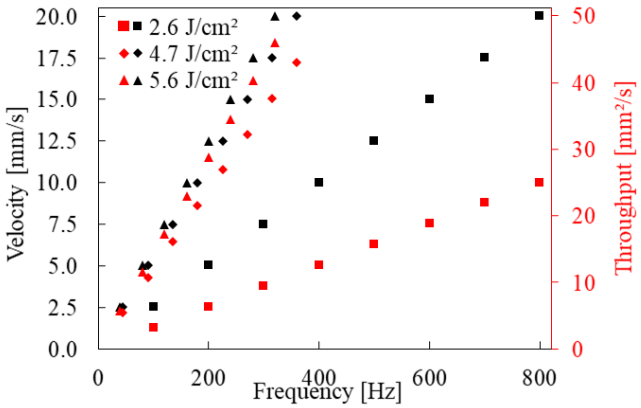

Fig. 5 Velocity and throughput of different laser fluence levels depending on the frequency

with an increase in the pulse frequency, the gaps between the individual pulses decreased, as expected. Particularly, for the surface treated at 50 Hz (Fig. 4c), on the overlapping areas the structures show a random texture due to the apparent re-melting of the material (areas in the image that appear darker). The calculated homogeneity of this structures is 0.81. Such featured random textures should be avoided for achieving high-quality and homogeneous structures. In case of the surface treated at 45 Hz (Fig. 4b), the structures feature smaller gaps compared to those fabricated at 37 Hz, and smaller areas of overlap compared to those fabricated at 50 Hz. The calculated homogeneity of the structures at a frequency of 45 Hz is 0.83 and is the highest that could be achieved in this case.

This means, that for a specific laser fluence and process velocity, the laser frequencies have to be readjusted (~20 % higher) for a better coverage of the total area of the metallic part. This was performed, using also optical microscopy for the laser fluences Φ of 2.6 J/cm² and 5.6 J/cm², obtaining frequencies of 100 and 40 Hz, respectively. These values differ ~30 and 25 % compared to the frequencies calculated using Eq. 1, respectively.

In order to get further information about the DLIP-robot arm process, the need linear velocities v as well as the possible process throughput that can be achieved were calculated. The last can be done by multiplying the length of the DLIP laser modified areas by the process velocity v. This has been plotted as function of the laser frequency f as well as the different used laser fluences as shown in Fig. 5.

In addition, the number of pulses needed per unit of distance (in the direction of the movement of the metallic parts and parallel to the interference lines) for each laser fluence

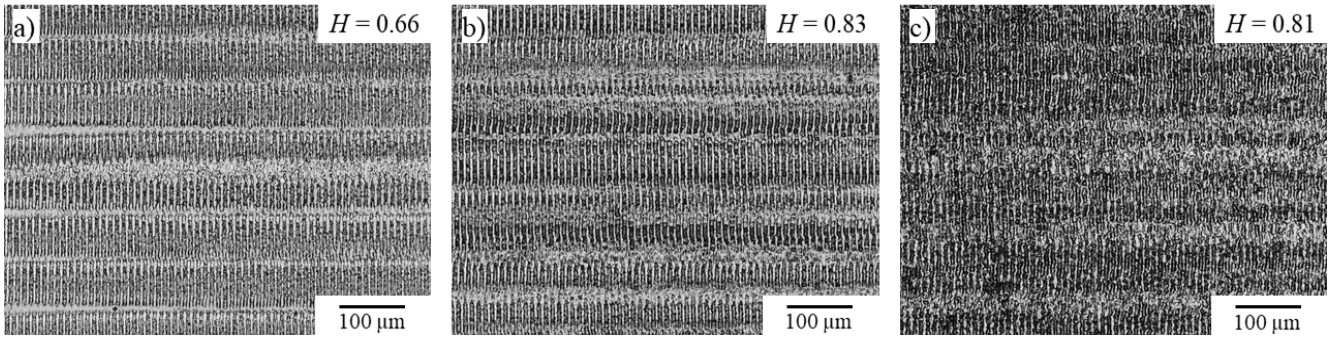

Fig. 4 Optical microscope images of DLIP structured stainless steel with Φ = 4.7 J/cm² and v = 2.5 mm/s at f = 37 Hz (a), f = 45 Hz (b) and f = 50 Hz (c).

was calculated from Eq. 2, obtaining 16 pulses/mm for Φ = 5.6 J/cm², 18 pulses/mm for Φ = 4.7 J/cm² and 40 pulses/mm for Φ = 2.6 J/cm².

$$n_{p\ per\ distance} = f/v. \quad (2)$$

Regarding the throughput, for the used velocity v of 2.5 mm/s, process velocities of 3.1, 5.4 and 5.8 mm²/s could be reached for Φ = 2.6 J/cm², 4.7 J/cm² and 5.6 J/cm², respectively.

These relative low values can be increased by employing higher velocities (and laser frequencies). On the other hand, due to the instabilities in the movement of the robot arm at higher velocities, it is unclear its impact in the surface homogeneity which was evaluated in a further experiment.

Thus, the surface homogeneity of DLIP-treated surfaces produced at velocities from 2.5 mm/s to 20 mm/s were evaluated. The laser fluence was set to 2.6 J/cm², 4.7 J/cm² and 5.6 J/cm², as in the previous experiments. Confocal microscopy images for velocities of 2.5 mm/s and 20 mm/s are presented as example in Fig. 6. The topographies shown exhibit a waviness or offset perpendicular to the structuring direction. This phenomenon occurs in all topographies and is therefore independent of the laser fluence and velocity parameters. It is attributed to the low precision of the robotic system (± 50 µm). The system oscillates inconsistently along the path between the predetermined points during structuring, resulting in a misalignment of the interference maxima of the DLIP optics.

The homogeneity (H) values, presented in Fig. 6, were calculated using the method described in [36,37], which utilizes the Gini coefficient as a statistical measure of equality. This approach objectively assesses the homogeneity of periodic surfaces, indicating that homogeneity is inversely proportional to the Gini coefficient.

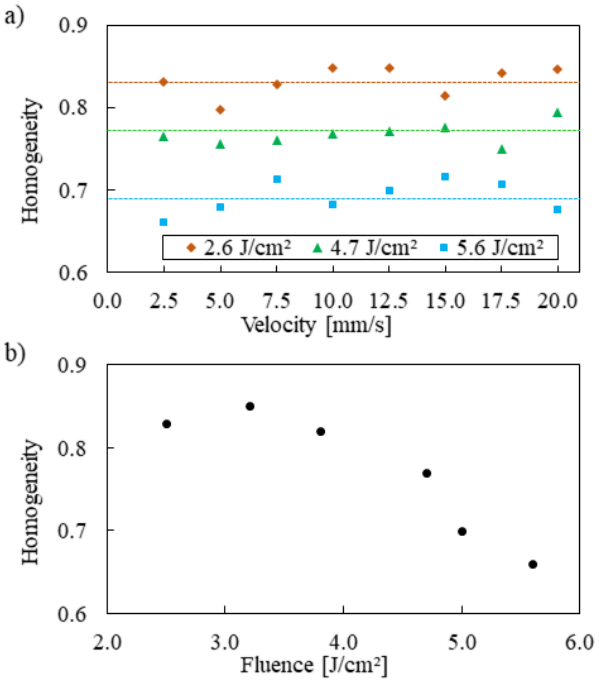

Fig. 7 Homogeneity of the structured surface depending on the laser fluence with increasing velocity (a) and fixed velocity of v = 2.5 mm/s (b).

As it can be seen, the homogeneity H does not significantly change depending on the process velocity v (the homogeneity H is indicated in Fig. 6 for each combination of process parameters. This effect is also shown for all used ve-

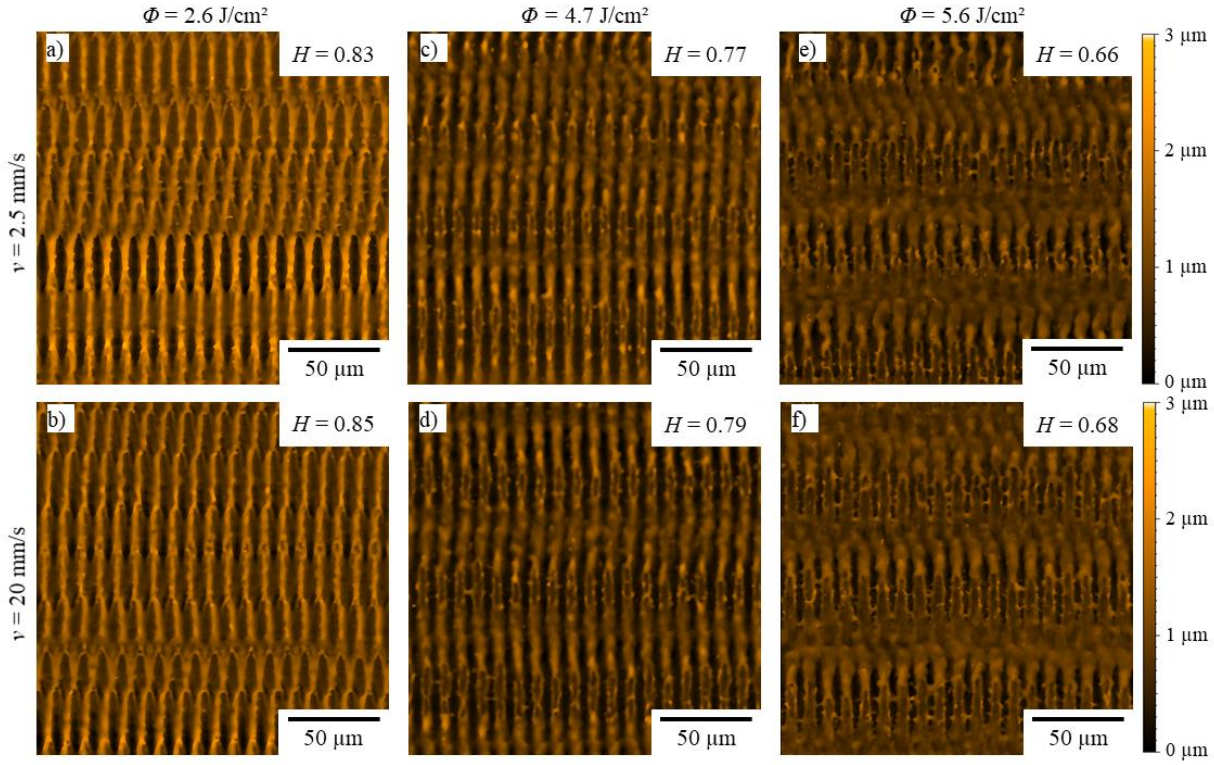

Fig. 6 Confocal microscope measurement of DLIP structured stainless steel for a velocity of v = 2.5 mm/s (a, c, e) and v = 20 mm/s (b, d, f) and a laser fluence of Φ = 2.6 J/cm² (a, b); Φ = 4.7 J/cm² and Φ = 5.6 J/cm² (e, f).

locities in Fig. 7a. For example, the H values of the structures fabricated with a laser fluence of 2.6 J/cm² (Fig. 6a, b) were 0.83 and 0.85 for velocities of 2.5 mm/s and 20 mm/s, respectively. For Φ = 4.7 J/cm², a similar trend was observed, with homogeneities H of 0.77 at 2.5 mm/s and 0.79 at 20 mm/s. This corresponds to a reduction of approximately ~7 % compared to the samples processed at the 2.6 J/cm². The same behaviour is observed independently of the used process velocity for Φ = 5.6 J/cm² (see Fig. 6e and 6f) with homogeneities H of 0.66 for 2.5 mm/s and 0.68 for 20 mm/s, representing a further reduction of approximately 14 %. The horizontal lines represent the mean value of the homogeneity depending on the applied laser fluence.

In consequence, it can be assumed that the changes in the calculated homogeneities are not related with the process velocity v, but depend on the used laser fluence as shown in Fig. 7a. This is exemplary illustrated for a constant velocity v of 2.5 mm/s in Fig. 7b. In particular, in the laser fluence range from 2.6 J/cm² to 4.7 J/cm², the homogeneity remains mostly unchanged (~0.77 – 0.85), while with a further increase of the laser fluence the homogeneity decreases. Especially from 4.7 J/cm², the homogeneity H drops significantly below 0.70. As explained above, this can be ascribed by large amounts of molten material flowing towards the valleys of the structures destroying the periodic pattern.

The above presented results indicate therefore, that increasing the process throughput does not affect the surface quality, but that the laser fluence has to be controlled. Thus, by keeping the laser fluence between 2.6 J/cm² and 4.7 J/cm², structure depths in the range of 0.83 to 1.25 µm can be reached, with homogeneity values over 0.77. In addition, the process throughput can be increased up to 25, 43 and 46 mm²/s, for laser fluences of 2.6, 4.7 and 5.6 J/cm² at a process velocity v of 20 mm/s (see Fig. 5).

The robot throughput is in the same magnitude as comparable DLIP processes in the µm range. For example, structures produced on flat surfaces were manufactured at a rate of 19 and 38 mm²/s respectively [13, 40]. In the case of structuring a cylindrical object, area rates of 95 mm²/s were achieved [15].

To increase the throughput, the length of the ablation area needs to be increased. This can be realised by adapting the optical system. Furthermore, this can be assisted by changing the beam profile from Gaussian to Top-Hat, as the beam intensity is homogeneous over the entire beam diameter and therefore deep structures are also present at the edges of the ablation area, thus increasing the hatch distance [41]. In addition to the length of the laser spot, velocity is a crucial factor. However, high acceleration and velocity result in significant dynamic loads within the system, potentially causing damage to both the optical and robotic components. In addition, the maximum axis rotation velocity of the robot can quickly be exceeded, which leads to the system to shut down.

Next, structures fabricated with the presented robot-based platform and with a conventional system based on a linear stage were compared. For this purpose, an optimum parameter set of Φ = 2.6 J/cm² and f = 100 Hz was selected for robot-based overlap-free structuring. In contrast, for the linear positioning system a parameter was set with Φ = 2.6 J/cm² and f = 5 kHz was chosen. Considering the width of the DLIP spot, the velocity was set to 100 mm/s, resulting in an overlap of 85 %. Confocal images of the structures fabricated using both setups are presented in Fig. 8. The structures fabricated with the linear-stage system exhibit a homogeneity of 0.95, whereby those produced by the robot-based platform have a homogeneity of 0.83. This difference can be explained due to the higher precision in the movement of linear stage (± 2.5 µm) compared to the robot-system (± 50 µm), as previously described. Furthermore, the mean structure depth for the linear-stage fabricated structures was 2.40 µm, which is also higher than the mean structure depth of 1.17 µm fabricated by means of the robot. The precise overlapping of the pulses means that a surface segment receives several pulses in a sequence. This multiple ablation

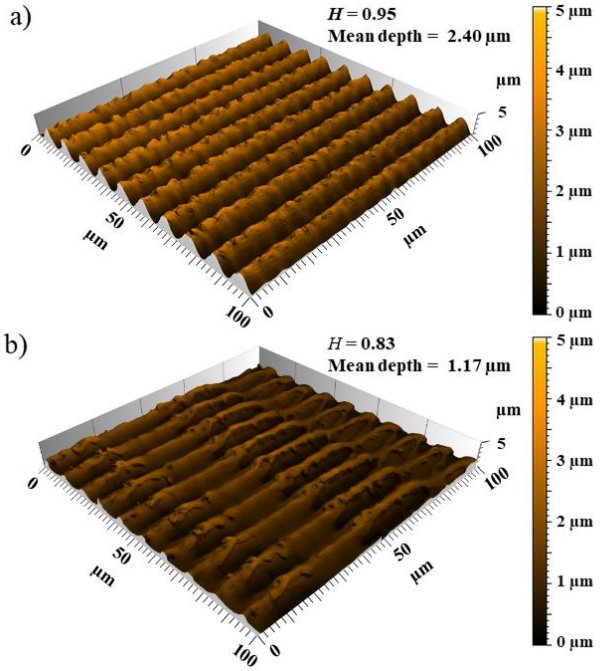

Fig. 8 Confocal microscope measurements of DLIP structured stainless steel using linear system (a) and robot system (b).

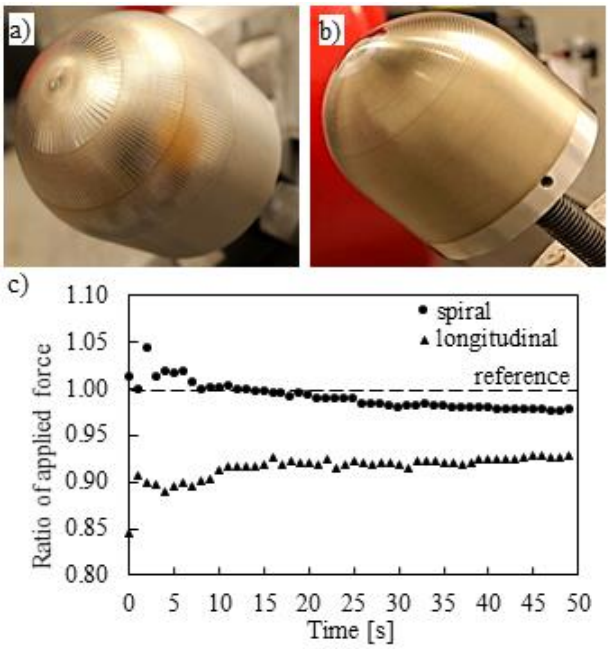

Fig. 9 Picture of longitudinal (a) and spiral (b) structured punches; Force ratio over time for longitudinal and spiral structured punches (c)

creates deeper grooves, which is not the case for robot-based overlap-free structuring.

The surface rates of both systems also differ significantly. For instance, the structures that were fabricated using the linear-stage system permitted to reach a throughput of 125 mm²/s, whereas the robot-based structuring was conducted at 3 mm²/s. This is attributed to the significantly higher linear velocity, which can only be achieved with the linear-stage system. Despite these significant differences in throughput, complex freeform surfaces of heavy parts can only be structured using the robotic system due to needed degree of freedom.

To investigate the feasibility of robot-based DLIP structuring on 3D parts, punches made of mild steel that are typically used for sheet forming were processed. The punches were locked in a two-axis positioner, which handled the rotary movement of the parts. The parameters $\Phi = 2.6$ J/cm² at $v = 2.5$ mm/s and $f = 100$ Hz were chosen for the structuring process due to their associated high structure homogeneity ($H > 0.83$) and practical feasibility, due to limitation of the maximum rotational velocity of the additional axis. Two strategies were pursued in the path planning, being longitudinal and spiral. For longitudinal structuring, individual tracks were fabricated along the surface parallel to the axis of rotation. The tracks converged at the tip of the punch. For spiral structuring, a single track was generated along the surface of the punch, which led helically to the tip. In Fig. 9a and 9b, photographs of the DLIP structured punches using the longitudinal and spiral approaches, respectively are shown. A third punch remained unstructured as a reference. Forming benchmark tests with aluminium sheets (0.9 mm thickness) were then carried out on a sheet metal press. The results of the structured punches were compared with the non-structured punch. The ratio of the applied forces (compared to the unstructured reference, denoted with the dashed line at 1.00) is shown in Fig. 9c.

The longitudinal structures correspond to parallel sliding of the punch, while the spiral structures are perpendicular to the sliding direction. As observed, punches structured with both strategies required less force than the non-structured punch. This effect can be attributed to a reduction in the friction coefficient due to the decreased contact area in the tribological system induced by the periodic structured surfaces [42]. Moreover, the parallel sliding direction requires significantly less force than the perpendicular sliding direction. However, studies show that structures perpendicular to the sliding direction exhibit a low coefficient of friction (COF), which is the opposite of our findings. In the case of perpendicular sliding, individual grooves act as repositories for wear particles, decreasing the COF [42,43]. Few studies report a low COF in the parallel sliding direction [44,45]. The simulation presented in [45] shows significantly higher contact stresses at the edges of the grooves in a perpendicular sliding direction. This can lead to a reduction in the COF due to an increase in the generation of wear particles. Finally, the obtained results show that the tribological performance of the forming tools can be enhanced even if the produced line-like structures have a homogeneity of 0.83.

4. Conclusions

Direct Laser Interference Patterning in combination with an industrial robot was used for the first time to texture metallic surfaces. As the ns-laser module and DLIP optics were both attached directly onto the robot arm, the degrees of freedom for the process are significantly enhanced, which enables an expansion of the fields of application for this process.

A new structuring strategy was developed in order to fabricate homogeneous structures. Individual pulses were placed side by side, because pulse overlapping reduced the texture uniformity due to the inaccuracy of the robot. Furthermore, a process window for laser fluence, frequency and velocity was identified in which homogeneous structures can be fabricated. The maximum throughput of 46 mm²/s at a velocity of 20 mm/s was also identified.

A comparison with a conventional linear stage system showed that the presented approach exhibited significantly lower throughput as well as less homogeneous structures. Nonetheless, this method permitted to process complex 3D surfaces that were previously unattainable using DLIP in combination with conventional linear stage systems.

Finally, punches with different structuring path strategies were fabricated with the parameters $\Phi = 2.6$ J/cm², $v = 2.5$ mm/s and $f = 100$ Hz. The applied force could be reduced by up to 10 % compared to the non-structured punch for the longitudinal structuring strategy.

Acknowledgments

This project was funded by the Federal Ministry for Economic Affairs and Climate Action (BMWK) on the basis of a decision by the German Bundestag.

References

[1] D. Sola, C. Lavieja, A. Orera, and M. J. Clemente: Opt. Laser Eng., 106, (2018) 139.
[2] S. Alamri and A. F. Lasagni: Opt. Express, 25, (2017) 9603.
[3] M. G. Holthaus, L. Treccani, and K. Rezwan: J. Eur. Ceram., 31, (2011) 2809.
[4] E. Shakhno, Q. Nguyen, D. Sinev, E. Matvienko, R. Zakoldaev, and V. Veiko: Nanomater., 11, (2021) 1.
[5] M. Bieda, C. Schmädicke, A. Wetzig, and A. F. Lasagni: Met. Mater. Int., 19, (2013) 81.
[6] L. Guo, H. Jiang, R. Shao, Y. Zhang, S. Xie, J. Wang, X. Li, F. Jiang, Q. Chen, T. Zhang, and H. Sun: Carbon, 50, (2012) 4.
[7] T. Kondo, S. Matsuo, S. Juodkazis, V. Mizeikis, and H. Misawa: Appl. Phys. Lett., 82, (2003) 2758.
[8] S. Alamri, F. Fraggelakis, T. Kunze, B. Krupop, G. Mincuzzi, R. Kling, and A. F. Lasagni: Matererials, 12, (2019) 1018.
[9] Y.-R. Wang, S. M. Olaizola, I. S. Han, C.-Y. Jin, and M. Hopkinson: Opt. Express, 28, (2020) 32529.
[10] H. Kasem, O. Stav, P. Grützmacher, and C. Gachot: Lubricants, 6, (2018) 3.
[11] L. G. Zschach, R. Baumann, F. Soldera, C. Mendez, S. Apelt, U. Bergmann, and A. F. Lasagni: Adv. Mat. Interfaces, 10, (2023) 36.
[12] P. Braun, P. Grützmacher, L. Frohnapfel, F. Mücklich, and K. Durst: Appl. Surf. Sci., 613, (2023) 155786.

[13] A. Peter, A. Lutey, S. Faas, L. Romoli, V. Onuseit, and T. Graf: Opt. Laser Technol., 123, (2020).
[14] C. He, K. Vannahme, and A. Gillner: J. Laser Micro/Nano Eng., 14, (2019) 95.
[15] M. Soldera, Q. Wang, F. Soldera, V. Lang, A. Abate, and A. F. Lasagni: Adv. Eng. Mater., 22, (2020) 4.
[16] Y. Ma, J. H. Park, S. J. Lee, J. Lee, S. Cho, and B. S. Shin: Int. J. Precis. Eng., 10,1, (2023).
[17] V. Furlan, A. Demir, G. Pariani, A. Bianco, and B. Previtali: EUSPEN, 49, (2018).
[18] L. Pongratz and K. Vannahme: Proc. SPIE, 11674, (2021) 116740P.
[19] F. Kuisat, F. Rößler, and A. F. Lasagni: Adv. Eng. Mater., 23, (2021) 5.
[20] T. T. Tung, N. Van Tinh, D. T. Phuong Thao, and T. V. Minh: Results in Engineering, 18, (2023).
[21] Y. Lin, H. Zhao, and H. Ding: Robot. Comput. Integr. Manuf., 48, (2017) 59.
[22] K. Wu, J. Li, H. Zhao, and Y. Zhong: Appl. Sci., 12, (2022) 8719.
[23] V. Lang, T. Roch, and A. F. Lasagni: Laser-based Micro-Nano. Process. X, 9736, (2016) 97360.
[24] F. Ränke, R. Baumann, B. Voisiat, and A. F. Lasagni: Mater. Lett. X, 14, (2022).
[25] A. F. Lasagni, T. Kunze, T. Roch, V. Lang, A. Gärtner, A. Rank, D. Günther, and M. Bieda: SPIE newsroom, (2016).
[26] B. Henriques, D. Fabris, B. Voisiat, A. R. Boccaccini, and A. F. Lasagni: Adv. Funct. Mater., 34, 2, (2024) 2307894.
[27] M. El-Khoury, M. Seifert, S. Bretschneider, M. Zawischa, T. Steege, S. Alamri, A. F. Lasagni, and T. Kunze: Mater. Letters, 303, (2021) 130284.
[28] H. Czichos and K.-H. Habig: Tribologie-Handbuch, (2010).
[29] A. Jarfors, S. J. Castagne, A. Danno, and X. Zhang: Technol., 5, 1, (2017) 3.
[30] T. Trzepieciński and Ľ. Kaščák: Technologia i Automatyzacja Montażu, 37, (2022).
[31] D. Buckley and K. Miyoshi: Wear, 100, (1984) 333.
[32] H. Czichos, S. Becker, and J. Lexow: Wear, 135, (1989) 171.
[33] K. Holmberg, H. Ronkainen, and A. Matthews: Ceram. Int., 26,7 (2000) 787.
[34] V. Weihnacht, A. Brückner, and S. Bräunling: Vakuum Forsch. Prax., 20, (2008) 3.
[35] T. Jähnig and A. F. Lasagni: Ind. Lubr. Tribol., 72, (2020) 1001.
[36] B. Lechthaler, C. Pauly, and F. Mücklich: Sci. Rep., 10, (2020) 14516.
[37] M. Soldera, C. Reichel, F. Kuisat, and A.F. Lasagni: J. Laser Mirco/Nano Eng., 17, 2, (2022) 81.
[38] B. Voisiat, C. Zwahr, and A. F. Lasagni: Appl. Surf. Sci., 471, (2019) 1065.
[39] F. H. Rajab, Z. Liu, and L. Li: Appl. Surf. Sci., 427, (2018) 1135.
[40] M. El-Khoury, B. Voisat, T. Kunze, and A. F. Lasagni: Materials, 15, (2022) 591.
[41] S. Fang, L. Llanes, S. Klein, C. Gachot, A. Rosenkranz, D. Bähre, and F. Mücklich: IOP Conf. Ser: Mater. Eng., 258, (2017) 012006.
[42] C. Gachot, A. Rosenkranz, R. Buchheit, N. Souza, and F. Mücklich: Appl. Surf. Sci., 367, (2016) 174.
[43] J. Wang, W. Xue, S. Gao, S. Li, and D. Duan: Wear, 486, (2021) 204079.
[44] T. Roch, V. Weihnacht, H.J. Scheibe, A. Roch, and A. F. Lasagni: Diam. Relat. Mater., 33, (2013) 20.
[45] S. Yuan, W. Huang, and X. Wang: Tribol. Int., 44, (2011) 9.

(Received: June 4, 2024, Accepted: December 9, 2024)